

An all-sky catalog of solar-type dwarfs for exoplanetary transit surveys

V. Nascimbeni,^{1,2*} G. Piotto,^{1,2} S. Ortolani,^{1,2} G. Giuffrida,^{3,4} P. M. Marrese,^{3,4} D. Magrin,² R. Ragazzoni,² I. Pagano,⁵ H. Rauer,^{6,7} J. Cabrera,⁶ D. Pollacco,⁸ A. M. Heras,⁹ M. Deleuil,¹⁰ L. Gizon^{11,12} and V. Granata^{1,2}

¹*Dipartimento di Fisica e Astronomia, “G. Galilei”, Università degli Studi di Padova, Vicolo dell’Osservatorio 3, 35122 Padova, Italy*

²*INAF – Osservatorio Astronomico di Padova, vicolo dell’Osservatorio 5, 35122 Padova, Italy*

³*ASI – Science Data Center, Via del Politecnico snc, 00133 Rome, Italy*

⁴*INAF – Osservatorio Astronomico di Roma, via Frascati 33, 00040 Monteporzio Catone, Italy*

⁵*INAF – Osservatorio Astrofisico di Catania, via S. Sofia 78, 95123 Catania, Italy*

⁶*Institute of Planetary Research, German Aerospace Center, Rutherfordstrasse 2, 12489 Berlin, Germany*

⁷*Department of Astronomy and Astrophysics, Berlin University of Technology, Hardenbergstrasse 36, 10623 Berlin, Germany*

⁸*Department of Physics, University of Warwick, Coventry CV4 7AL, UK*

⁹*Scientific Support Office, Directorate of Science, European Space Agency, ESTEC/SCI-S,*

Keplerlaan 1, 2201 AZ Noordwijk, The Netherlands

¹⁰*Aix Marseille Université, CNRS, LAM (Laboratoire d’Astrophysique de Marseille) UMR 7326, F-13388 Marseille, France*

¹¹*Max-Planck-Institut für Sonnensystemforschung, Justus-von-Liebig-Weg 3, 37077 Göttingen, Germany*

¹²*Institut für Astrophysik, Georg-August-Universität, Friedrich-Hund-Platz 1, 37077 Göttingen, Germany*

Submitted N/A; Accepted N/A; compiled: 2018/11/06 at 23:45:06.

ABSTRACT

Most future surveys designed to discover transiting exoplanets, including TESS and PLATO, will target bright ($V \lesssim 13$) and nearby solar-type stars having a spectral type later than F5. In order to enhance the probability of identifying transits, these surveys must cover a very large area on the sky, because of the intrinsically low areal density of bright targets. Unfortunately, no existing catalog of stellar parameters is both deep and wide enough to provide a homogeneous input list. As the first Gaia data release exploitable for this purpose is expected to be released not earlier than late 2017, we have devised an improved reduced-proper-motion method to discriminate late field dwarfs and giants by combining UCAC4 proper motions with APASS DR6 photometry, and relying on RAVE DR4 as an external calibrator. The output, named UCAC4-RPM, is a publicly-available, complete all-sky catalog of solar-type dwarfs down to $V \simeq 13.5$, plus an extension to $\log g > 3.0$ subgiants. The relatively low amount of contamination (defined as the fraction of false positives; $< 30\%$) also makes UCAC4-RPM a useful tool for the past and ongoing ground-based transit surveys, which need to discard candidate signals originating from early-type or giant stars. As an application, we show how UCAC4-RPM may support the preparation of the TESS (that will map almost the entire sky) input catalog and the input catalog of PLATO, planned to survey more than half of the whole sky with exquisite photometric precision.

Key words: catalogs – methods: statistical – stars: planetary systems – stars: statistics – stars: solar-type

1 INTRODUCTION

Although a couple of thousand exoplanets have been discovered, the general picture on their structure, formation and

evolution is still far from being complete. Putting things in context requires a more detailed analysis of individual systems than is currently achievable. This includes, for instance, the estimate of accurate stellar masses and ages through asteroseismology and a detailed characterization of the planetary atmospheres through spectroscopy. Both these tasks

* E-mail: valerio.nascimbeni@unipd.it

require high S/N, and are feasible only when targeting planets hosted by nearby and bright stars, which have been very rare indeed so far. In the next years, two cornerstone, space-based missions that will photometrically detect and partially characterize planetary systems around bright stars will be launched: TESS (Ricker et al. 2015), a NASA Explorer mission selected for launch in 2017-2018; and PLATO (Rauer et al. 2014), a medium-class mission selected for ESA’s M3 launch opportunity (2022-2024).

Aside from being bright ($V \lesssim 13$), the most promising targets for exoplanetary science are solar-type stars, i. e., main-sequence stars later than spectral type F5, which could include moderately-evolved subgiants following a broader definition. As a magnitude-limited sample of field stars is dominated by distant (and intrinsically bright) giants and early-type stars, the only way to access a large sample of bright, nearby solar-type stars (as required by transit exoplanet search surveys) is to dramatically increase the covered sky area up to a significant fraction of the whole celestial sphere. In this case, the selection of a homogeneous target list requires the deepest all-sky stellar classification ever attempted, able to assign at least a spectral type and luminosity class to every star brighter than $V = 13$. This should be regarded as a minimal requirement for carrying out the target selection task. Previous experience from the CoRoT and Kepler space missions (Deleuil et al. 2009; Brown et al. 2011) has shown that detailed knowledge of the stellar parameters of the targets (such as effective temperature T_{eff} , surface gravity $\log g$, metallicity [M/H], stellar mass and radius R_* , M_* , age, etc.) along with the identification and characterization of the background stars (Deleuil et al. 2006) helps to prioritize the targets, and makes the follow-up and the rejection of false alarms much more efficient.

The Gaia mission¹ (Perryman et al. 2001), launched in 2013 and currently collecting data, is expected to play a fundamental role in the target selection by performing an unprecedented ultra-high-precision astrometric survey of nearly every source brighter than $V \simeq 20$, along with low-resolution spectrophotometry and radial velocities. An intermediate catalog which includes stellar parameters from spectrophotometry is expected to be released at the end of 2017². However, we should keep in mind that i) the Gaia stellar classification will be affected by crowding in the densest fields (Bailer-Jones et al. 2013; Recio-Blanco et al. 2016); ii) there will be some degeneracy among certain parameters, such as temperature and interstellar extinction (Straizys et al. 2006; Bailer-Jones 2010; Bailer-Jones et al. 2013); iii) other astronomical catalogs (for instance, X/UV/IR/narrow-band photometry and activity diagnostics) will be very complementary to the Gaia measurements; iv) space missions (e.g. TESS) and ground-based surveys which are presently in development may require a preliminary target list before 2017, for the performance analysis, to optimize the observing strategy, to fine-tune the spacecraft design, and to begin implementing the foreseen additional observations and coordinated follow-up programs.

In this paper, we first introduce the basic problem of attempting a large-scale stellar classification by relying only

on wide-band photometry and proper motions (Section 2), and review the existing techniques and catalogs designed for that purpose (Section 3). After showing that a new approach has to be devised, in Section 4 we describe how we compiled a brand-new all-sky catalog of FGK dwarfs and subgiants, called UCAC4-RPM. We include a detailed description of the catalogs used as input, the grid-based algorithm exploited to define appropriate selection criteria, and the cross-matching procedure used to estimate the contamination and completeness of the resulting sample. Finally, in Sections 5 and 6 we discuss how UCAC4-RPM can be exploited by the ongoing or forthcoming space- and ground-based transit surveys, and how it could be extended and complemented in the future.

2 THE BASIC PROBLEM

The most reliable stellar classification is provided by spectra and trigonometric parallaxes from which it is possible to extract the basic parameters of the stellar atmosphere (T_{eff} , $\log g$, [M/H]) and its distance and absolute magnitude in a relatively straightforward way. Once these parameters are known, we can use stellar evolutionary models to derive other important physical quantities such as the radius R_* , the mass M_* , and the age of the star. Spectroscopy and high-precision astrometry are time-consuming. Alternative approaches, based on narrow-band photometry (Árnadóttir et al. 2010) are more suited to wide-field surveys (at a price of lower accuracy), but they are still too costly in terms of observing time.

Until Gaia releases accurate parallaxes, it is not feasible to characterize hundreds of thousands of stars on an extremely large field of view with the techniques mentioned above. The only available, accurate all-sky classifications of this kind are limited to sources at $V \lesssim 8$ or even brighter, based on spectroscopic surveys (HD, MK classifications; Morgan & Keenan 1973; Skiff 2014), narrow-band surveys (Geneva-Copenhagen; Nordström et al. 2004) or the space-based Hipparcos catalog (Perryman & ESA 1997; van Leeuwen 2007). At the present time, we must rely on the only available catalogs that reach the $V \simeq 13$ limit: wide-band photometric catalogs (both in the visible and in the near-infrared) and ground-based astrometric catalogs, which are accurate enough to provide good proper motions, but not trigonometric parallaxes. In what follows we present the difficulties and limitations of exploiting these sub-optimal data for stellar classification purposes.

For a detailed review of the main standard photometric systems, see Bessell (2005). A summary of calibrated broad-band colors and physical properties of typical main sequence, solar-metallicity dwarfs is given in Table 15.7-15.8 by Cox (2000). A revised and constantly updated version of that table is maintained by E. Mamajek³ (Pecaut & Mamajek 2013).

¹ <http://sci.esa.int/gaia/>

² <http://www.cosmos.esa.int/web/gaia/release>

³ http://www.pas.rochester.edu/~emamajek/EEM_dwarfUBVIJHK_colors_Teff.txt

2.1 Wide-band photometry

Using wide-band photometry to derive stellar parameters is a challenging task for many reasons. First of all, over most of the visible spectrum, the expected differences in color between cool stars of similar T_{eff} and spectral type (SpT), but different surface gravity $\log g$ and metallicity $[\text{Fe}/\text{H}]$, are at most a few tenths of a mag, even when exploiting custom-designed narrow- or intermediate-band filters (Zdanavičius 2005, see their Fig. 1c-1f). When the spectral energy distribution of those stars is integrated over the wavelength ranges of a typical wide-band photometric system ($\Delta\lambda \approx 1000 \text{ \AA}$) the differences fade to only a few hundredths of mag. A notable exception is in the spectral region bluer than the “Balmer jump”, which is sampled by both the Johnson U and the SDSS u' filters (Zdanavičius 1998, 2005). Unluckily, these magnitudes are the most difficult to measure and calibrate from the ground, due to atmospheric effects, standardization issues and low instrumental sensitivity (Bessell 2005). So far, no all-sky, deep catalog of U/u' magnitudes is available.

Even more importantly, wide-band photometric classifications are known to be highly degenerate on some stellar parameters, such as metallicity and gravity; see for instance the example reported by Belikov & Röser (2008), and Fig. 1 of this paper. By using a B , V , J two-color diagram, it is not possible to discriminate between metal-poor dwarfs and solar-metallicity giants, both of G spectral type. F, G and K stars are expected to dominate a magnitude-limited sample at $V < 13$, and they are located in the color-magnitude diagram (CMD) and color-color diagram region where most degeneracy occurs. A further source of degeneracy is interstellar reddening, which is not negligible in a magnitude-limited sample of stars at low and intermediate Galactic latitudes. In particular, $E(B - V)$ (or A_V) and T_{eff} are degenerate: a distant, hot star can be easily misclassified as a closer and cooler star. To a lesser extent, this also holds for near-infrared (NIR) photometry, and even when parallaxes and low-resolution spectra are available (Bailer-Jones 2010, 2011).

The most basic aim of an input catalog for transit surveys is to distinguish dwarfs from giants for the spectral types ranging from mid-F stars down to the late M ones. The most relevant spectral regions are therefore those sensitive to $\log g$. Aside from the optical ultraviolet (UV) wavelengths, the most prominent features are located on the continuum at 4000-4500 \AA (“G band”; mostly for the F-G spectral types) and at the MgI triplet/MgH absorption feature at 5150-5200 \AA (mostly for G-K spectral types, as demonstrated also by Teig 2008). Most narrow- and intermediate-band photometric systems developed for stellar classification purposes, as well as the G_{red} and DDO51 filters originally designed for the Kepler Input Catalog survey (KIC; Batalha et al. 2010; Brown et al. 2011) are tailored on these spectral features.

As for wide-band photometry, we note that the three above-mentioned features fall roughly inside the Johnson U , B , V bands, though their contribution is greatly diluted by the bandwidth effect, and it never exceeds a few hundredths of magnitude on the $B - V$ color. Cousins R_c and I_c bands are relatively insensitive to $\log g$, except for the spectral class M. Results from synthetic photometry applied to M dwarfs

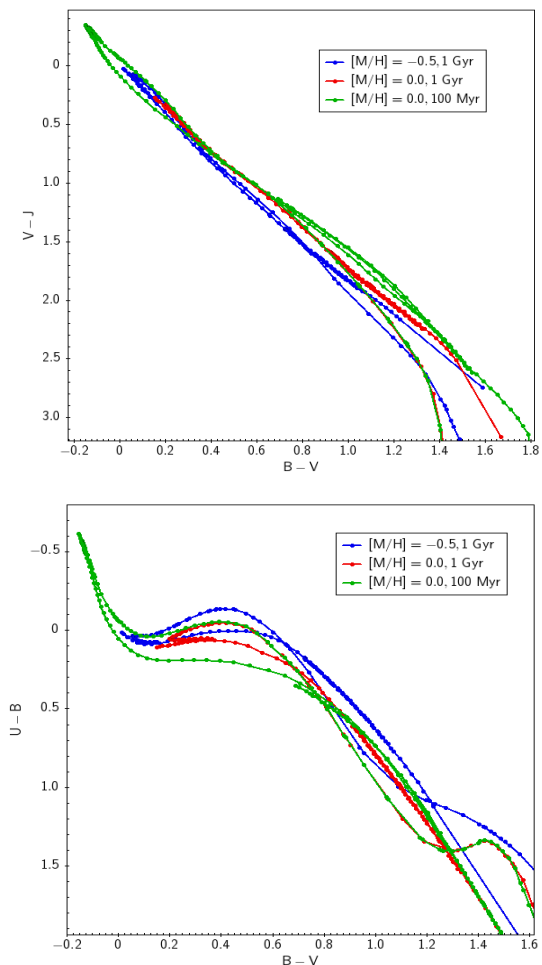


Figure 1. Synthetic $(V - J)$ vs. $(B - V)$ (upper panel) and $(U - B)$ vs. $(B - V)$ (lower panel) color-color diagrams illustrating how retrieving a unique solution for stellar parameters from wide-band photometry can be a complicated task. PARSEC isochrones (PADova and TRIeste Stellar Evolution Code; Bressan et al. 2012) are coded with different colors: $[\text{M}/\text{H}] = 0.0$ and 1 Gyr age (green), $[\text{M}/\text{H}] = 0.0$ and 0.1 Gyr (blue), $[\text{M}/\text{H}] = -0.5$ and 1 Gyr (red). There clearly are multiple cases of degeneracy where isochrones with different metallicities and ages intersect each other, in particular in the FGK region.

should be approached with caution, as the theoretical uncertainties of their atmospheric opacities result in large differences between calculated and observed SEDs (Zdanavičius 2005). NIR wide-band photometry, that is carried out in the JHK or JHK_s bands by ground-based surveys (such as 2MASS; Skrutskie et al. 2006), is particularly effective in discriminating gravity effects on very late spectral types. $H - K$ or $H - K_s$ colors, for instance, can differ by a few tenths of mag between M dwarfs and M giants (Lépine & Shara 2005). This technique can be extended to late K stars. However, NIR color effects become smaller and very degenerate for earlier types such as F and G. On the other hand, NIR colors are less affected by interstellar extinction, and they can be advantageous on fields at low Galactic latitudes, where reddening effects are not negligible.

2.2 Proper motions

Proper motions, which are provided with a typical accuracy of a few mas/yr by existing catalogs such as those from the Tycho-2 (Høg et al. 2000) and UCAC4 (Zacharias et al. 2013) surveys, proved to be helpful in discriminating dwarfs from giants when combined with photometric colors. The so-called Reduced Proper Motion technique (RPM) exploits a combination of proper motions μ_α, μ_δ and apparent magnitude m as a statistical proxy to the target distance. By crudely assuming that all field stars share the same absolute velocity pointed towards a random direction on the sphere, one concludes that the quantity

$$\text{RPM}(m) = m - 5 + 5 \log \sqrt{(\mu_\alpha \cos \delta)^2 + \mu_\delta^2}, \quad (1)$$

called *reduced proper motion* is statistically approximating the absolute magnitude of the stars plus a constant offset⁴. RPM diagrams (RPMD) are therefore similar to CMDs smeared along the vertical axis, and, as such, can be exploited to select specific types of stars.

RPMs are very effective in selecting main-sequence dwarfs among bright ($V \leq 11$) stars belonging to late spectral types (K-M), as demonstrated by Gould & Morgan (2003) and Gontcharov (2009), among others. On fainter stars, and for F and G spectral types, the RPM technique is less effective, and a larger fraction of false positives is expected (Gould & Morgan 2003). RPMs, by themselves, cannot provide stellar parameters other than a very rough estimate of the absolute magnitude or SpT. In addition, selection cuts based on proper motions have to be devised with care, as the resulting sample could be biased in subtle ways toward thick disk or halo targets, which share a higher intrinsic velocity (Lépine & Shara 2005) and different metallicity.

3 PREVIOUS CLASSIFICATION ATTEMPTS

Beginning in the 2000s, with the advent of accurate all-sky catalogs such as Hipparcos, Tycho-2, and 2MASS, some authors have tried to extract stellar parameters using only wide-band photometry and proper motions. Some were driven by the need to extract a target list for exoplanet searches (e.g., Ammons et al. 2006 for the NHK radial velocity survey, Gould & Morgan 2003 for generic transit surveys). Others were trying to provide an all-sky calibration for the *ugriz* passbands (Ofek, 2008; Pickles & Depagne, 2010), to develop a general method to classify Galactic stellar populations (Bilir et al., 2006; Belikov & Růser, 2008), or to distinguish particular classes of stars, such as M dwarfs from M giants (Lépine & Shara 2005). Most of these works exploit the same input catalogs with different algorithms. Usually they are based on Tycho-2 B_T, V_T and 2MASS JHK_s magnitudes, as they provide uniform, precise all-sky photometry over pass bands that contain useful information on $[M/H]$ and $\log g$ (See Section 2). Proper motions, when needed, are also extracted from Tycho-2. Unfortunately, most photometric classifications are limited to about $V \leq 11$ by the completeness limit of Tycho-2. While 2MASS provides very

good photometry ($\sigma < 0.05$ mag) down to $V \sim 15$ and Tycho-2 proper motions are also well complemented by the UCAC survey for stars brighter than $V \sim 15$, no reliable source of visual magnitudes was available for $V \geq 11$ on the whole sky until recently. In what follows we shortly review a few previous classification attempts which are most relevant to our purposes.

3.1 Template matching techniques

Ofek (2008) matched the 2MASS and Tycho-2 catalogs, and fitted the resulting $B_T V_T JHK_s$ magnitudes with a set of library spectra computed by Pickles (1998). A best-fit template was then assigned to each star, and a set of SDSS *griz* synthetic magnitudes was calculated for each template to construct an all-sky catalog of *griz* magnitudes for calibration purposes. Though not specifically designed to derive stellar parameters, this work yielded spectral types and luminosity classes for ~ 1.56 millions Tycho-2 entries. On a subset range of spectral types, metal rich vs. metal poor stars are also differentiated. For unknown reasons, stars having $\delta \simeq 4^\circ, 54^\circ \leq \delta \leq 59^\circ, \delta \geq 80^\circ$ are lacking.

Pickles & Depagne (2010) extended the work done by Ofek by fitting updated spectral templates on a larger set of stellar magnitudes, having complemented the Tycho-2/2MASS $B_T V_T JHK_s$ with the photographic R_N magnitudes from USNO-B1.0 (through the NOMAD catalog, compiled by Zacharias et al. 2005). Cuts were performed on 2MASS $J - H, H - K_s$ colors and Tycho-2 proper motions, attempting to distinguish giants from dwarfs when the spectral template χ^2 -fitting is unable to do it. For our purposes, both the Ofek (2008) and Pickles & Depagne (2010) classifications should be handled with caution. Interstellar reddening is not accounted for, and this is known to let many distant, hot giants to be misclassified as cool dwarfs. If one only selects $V < 11, \text{SpT} > \text{F5}$ stars, the resulting sample is strongly concentrated towards the Galactic disk, and this is even more striking when selecting only K and M dwarfs, which, at bright magnitudes, should be isotropically distributed on the sky. Moreover, K and M stars dominate the sample along the Galactic plane, while A, F and G stars are expected to do so in a magnitude-limited sample. Summarizing, the classification algorithms above are not to be trusted when working at low Galactic latitudes ($b < 20^\circ$).

A more complex approach to template-matching stellar classification is that attempted by Belikov & Röser (2008), who defined a set of custom extinction-free indexes Q_{123} calibrated on the Tycho-2/2MASS photometric systems ($B_T V_T JHK_s$). An interval-cluster analysis was then applied to extract $T_{\text{eff}}, \log g, [M/H]$ by fitting Kurucz models to Q on the whole Tycho-2/2MASS set, after the algorithm has been trained on a subset having known spectroscopic parameters. Adopting Q indexes also allowed the authors to constrain the extinction A_V . As a result, bright, nearby dwarfs are homogeneously distributed, except for a few sky regions where very high or anomalous extinction occurs (e. g., the Ophiucus cloud or at very low b).

3.2 Proper-motion-based techniques

The RPM approach, introduced in Section 2.2, was first pioneered by Kapteyn & van Rhijn (1920) and Hertzsprung

⁴ Some authors give a slightly different definition of the RPM quantity, which differs only by an unessential constant.

(1922), and applied for the first time to the Tycho-2 catalog by Gould & Morgan (2003), purposely to select targets for transit searches. Since then, wider or improved approaches were attempted, the following one being the most relevant to our purposes.

Ammons et al. (2006) developed an entirely empirical method to identify metal-rich, low main-sequence stars as targets for N2K, a radial velocity search for hot Jupiters (Fischer et al. 2005). A training set made of 1000 F, G, and K stars with both high-resolution spectra from Valenti & Fischer (2005) and photometry from Tycho-2/2MASS was employed to fit polynomials and spline functions to broad-band colors extracted from $B_T V_T JHK_s$ magnitudes and Tycho-2 proper motions. Those analytical functions were then interpolated on all the well-measured Tycho-2 sources with a χ^2 -minimization procedure, in order to derive distances and temperatures. For a selected subset of 354 822 FGK dwarfs, $[M/H]$ and probability of multiplicity were also derived with the same technique, while T_{eff} was estimated with a finer polynomial function. On FGK dwarfs with photometric errors $\sigma_V < 0.05$ mag, the temperature and metallicity models give a standard error of 70 K and 0.14 dex, respectively. The binary model can remove 70% of doubles with $1.25 < M_1/M_2 < 3.0$ from a magnitude-limited sample of dwarfs at a cost of cutting 20% of the sample. This technique primarily uses the distance (and hence the absolute magnitude) as a proxy to discriminate dwarfs from giants. It fails when trying to directly estimate $\log g$. The main reasons are: 1) the physical processes that differentiate dwarfs from giants in photometry vary widely as a function of T_{eff} : a single polynomial or even a spline cannot be expected to capture all possible effects; 2) some rare kinds of stars are underrepresented by the Valenti & Fischer (2005) training set, namely, blue giants and cool red dwarfs. Though reddening is not taken into account, using proper motions to infer the distance minimizes the contamination of the sample by giants, even at low Galactic latitudes.

3.3 The contamination issue

The aim of our work is to select main-sequence dwarfs having a spectral type later than F5 (DLF5 hereafter), possibly also including moderately evolved subgiants within the same SpT range (DSL5F5 hereafter). Classification algorithms label catalog entries as positives (i.e., “good” targets which meet our requirements; P) or negatives (N), while the terms true (T) and false (F) refer to what these objects actually are. The four possible outcomes within this scheme are therefore TP, TN, FP, FN. Every classification technique which aims at selecting DLF5/DSL5F5 stars can unavoidably 1) fail at including some objects which are indeed DLF5/DSL5F5, that is it misses *true negatives*, and 2) include targets (mostly hot dwarfs, evolved giants or non-stellar objects) which are contaminants, otherwise called *false positives*. From here on, we define

- (i) *completeness* the fraction of true positives over the total number of true targets, $TP/(TP+TN)$;
- (ii) *contamination* the fraction of false positives over the total number of positives, $FP/(TP+FP)$.

Ideally, we are searching for a technique which outputs a complete sample with zero contamination.

The DSL5F5/DLF5 samples are usually defined in terms of spectral type and luminosity class (Section 1). Translating this definition into a new one based on a range of T_{eff} and $\log g$ would enable an easier, direct and more accurate comparison among different classification schemes. There is no general agreement in the literature on how to link stellar parameters to a given SpT, and second order effects, such as metallicity and ages, further complicate the problem. We define

- the main DSL5F5 sample as MS or post-MS stars having $T_{\text{eff}} < 6510$ K and $\log g > 3.0$;
- the DLF5 subset as MS stars having $T_{\text{eff}} < 6510$ K and $\log g > 3.5$.

The thresholds on T_{eff} and $\log g$ were set according to the empirical calibrations of the F5V SpT published on Cox (2000) and on literature data compiled by E. Mamajek⁵ and cross-matched with the PASTEL catalog of stellar spectroscopic parameters (Soubiran et al. 2010).

In order to assess the completeness and contamination of a sample selected by the existing classification algorithms, we matched catalogs by Ammons et al. (2006) and Ofek (2008) (hereafter AM06 and OF08; typical examples of RPM and template matching based techniques, respectively) with a reliable catalog of atmospheric parameters. To that purpose, we chose the fourth and most recent data release (DR4) of the spectroscopic survey RAVE (Steinmetz et al. 2006; Kordopatis et al. 2013). RAVE, Radial Velocity Experiment⁶ (Steinmetz et al. 2006), is a spectroscopy survey at $R \simeq 7000$ resolution, based at the Australian Astronomical Observatory, aiming at delivering accurate radial velocities (~ 1.5 km/s), atmospheric parameters and elemental abundances for about half a million stars in the Southern hemisphere. The RAVE sample is magnitude-limited at $I < 12$, although not complete.

The DLF5 and DSL5F5 subsets were extracted from the OF08 stars according to their “photometric” T_{eff} and $\log g$, following the definitions given above. As for the AM06 catalog, the authors provide a pre-selected subset of FGK main-sequence dwarfs, which we further trimmed at $T_{\text{eff}} < 6510$ K to obtain a pure DLF5 sample; no DSL5F5 sample can be straightforwardly extracted from AM06, because no direct information on $\log g$ is available from this work.

Now, let us focus on the DLF5 subsets of AM06 and OF08. Their distribution (red contours) is compared with that of the general field (black contours) and plotted in Fig. 2 as a function of their spectroscopic parameters T_{eff} , $\log g$ as tabulated in RAVE DR4, for both AM06 (left panel) and OF08 (right panel) input catalogs. Following our previous definition, contamination and completeness were estimated with respect to the fraction of stars falling outside the boundaries $\log g > 3.5$ and $T_{\text{eff}} < 6510$ K as given by RAVE. The resulting contamination spans ~ 25 -38% for AM06 and OF08, respectively, while completeness spans ~ 45 -66% (Table 1). Contaminants are mostly red giants for OF08, and are equally shared between red giants and earlier main-sequence types for AM06. We also did a similar estimation on the

⁵ https://www.pas.rochester.edu/~emamajek/IV_standards_PASTEL_logg.txt

⁶ <https://www.rave-survey.org/>

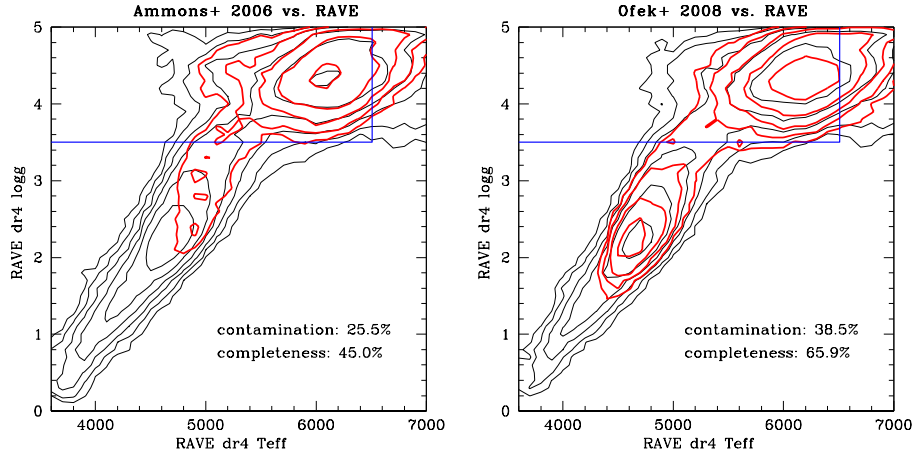


Figure 2. Effective temperature T_{eff} and surface gravity $\log g$ from RAVE DR4 for a subset of stars in common with the [Ammons et al. \(2006\)](#) (left panel) and [Ofek \(2008\)](#) (right panel) catalogs. The distributions of both the overall sample (black contour lines) and for DLF5 subsets (red contour) as classified by photometry alone are shown. The blue lines mark the boundaries $T_{\text{eff}} < 6510$ K, $\log g > 3.5$ which define the DLF5 sample; red sources outside this region are therefore classified as contaminants (see Section 3.3).

Table 1. Sky-averaged contamination and completeness of DLF5 and DSLF5 samples extracted from various stellar classification algorithms, by assuming the RAVE DR4 spectroscopic database as a reliable source of stellar parameters.

catalog	sample	subset	contamination	completeness	m_{lim}
Ammons et al. (2006)	DLF5 ⁽¹⁾	all-sky	25.5%	45.0%	$V < 11$ ⁽²⁾
Ofek (2008) ⁽³⁾	DSL5F5	all-sky	36.2%	71.8%	$V < 11$
Ofek (2008) ⁽³⁾	DLF5	all-sky	38.5%	65.9%	$V < 11$
Belikov & Röser (2008)	DLF5	all-sky	38.2%	— ⁽⁴⁾ %	$V < 11$
UCAC4-RPM (this work)	DSL5F5	all-sky	28.8%	79.9%	$f < 13.5$
UCAC4-RPM (this work)	DLF5	all-sky	27.7%	80.0%	$f < 13.5$
UCAC4-RPM (this work)	DSL5F5	$ b > 20^\circ$	28.0%	71.2%	$f < 13.5$
UCAC4-RPM (this work)	DLF5	$ b > 20^\circ$	27.5%	79.4%	$f < 13.5$
UCAC4-RPM (this work)	DSL5F5	$10^\circ < b < 20^\circ$	28.0%	83.7%	$f < 13.5$
UCAC4-RPM (this work)	DLF5	$10^\circ < b < 20^\circ$	27.9%	81.8%	$f < 13.5$
UCAC4-RPM (this work)	DSL5F5	$ b < 10^\circ$	28.3%	82.0%	$f < 13.5$
UCAC4-RPM (this work)	DLF5	$ b < 10^\circ$	28.0%	80.6%	$f < 13.5$

Notes. Contamination and completeness fractions are defined in Section 3.3. (1) the [Ammons et al. \(2006\)](#) catalog does not provide $\log g$; instead, a pre-compiled set of FGK dwarfs is available, from which we trimmed a DLF5 sample by imposing $T_{\text{eff}} < 6510$ K; no extension to DSL5F5 is possible. (2) the completeness limit of Tycho-2 is here assumed to be $V \lesssim 11$, though slightly depending on SpT and Galactic latitude. (3) the [Ofek \(2008\)](#) DLF5 and DSL5F5 sample are selected according to the best- χ^2 [Pickles \(1998\)](#) template. (4) The only part of the [Belikov & Röser \(2008\)](#) catalog which is available to us is just a subsample of FGK dwarfs; without knowing the exact composition of the initial sample it is possible to estimate the contamination but not the completeness.

[Belikov & Röser \(2008\)](#) catalog, which resulted in a $\sim 38.2\%$ contamination, very close to the OF08 result (Table 1). Considering that the vast majority of a magnitude-limited sample is composed of early-type and evolved giants, photometric classification techniques such these ones represent an acceptable starting basis for the target selection process.

Unfortunately, all the reviewed catalogs including OF08 and AM06 are magnitude-limited ($V \lesssim 11$) because they are based on Tycho-2. If we want to extend our classification to fainter stars ($V \lesssim 13$), while taking advantage of RAVE DR4 as a reliable external calibrator with the aim of improving both completeness and contamination, we must use different input catalogs and devise a new classification algorithm.

This is the main driver for the creation of our brand new all-sky catalog of DLF5 and DSL5F5 stars, hereafter named UCAC4-RPM.

4 THE UCAC4-RPM CATALOG COMPILATION

4.1 Input catalogs

We chose to adopt UCAC4 ([Zacharias et al. 2013](#)) as the starting point to build our new catalog. UCAC4 is a compiled, all-sky astrometric catalog designed to provide high-quality CCD positions and proper motions for targets fainter

than the limiting magnitude of Hipparcos and Tycho-2. The observations are designed to cover the $R = 7.5$ to 16.3 magnitude range, and were performed through one pass band at approx. 579–643 nm. Most observations were carried out in non-photometric conditions, but UCAC4 native magnitudes f_{mag} have been calibrated against Tycho-2 stars and systematic errors are constrained within 0.1 mag, and sometimes much better. Positional errors are between 15–20 mas for stars with $10 \lesssim V \lesssim 14$. UCAC4 is supplemented by proper motions and SuperCosmos (Hambly et al. 2001) and 2MASS NIR photometric data, as well as diagnostic flags. The proper motions of bright stars are based on about 140 catalogs, including Hipparcos and Tycho-2. Proper motions of faint stars are based on a re-reduction of early epoch SPM (van Altena 2011) data (at $-90^\circ < \delta < -10^\circ$) plus Schmidt plate data from the SuperCosmos project.

UCAC4 native magnitudes are complemented by the sixth data release (DR6) of the AAVSO Photometric All-Sky Survey⁷, (APASS; Henden & Munari 2014) in five filters: Johnson B and V , plus Sloan g , r , i . Once completed, APASS will cover the magnitude range between $V \simeq 10$ and $V \simeq 17$. It will conveniently link Tycho-2 to SDSS, plus cover the whole sky at the same depth of UCAC4. Johnson B and V were chosen to extend the Tycho-2 calibration to fainter magnitudes, while Sloan g' , r' , i' will homogeneously extend the much deeper SDSS, SkyMapper, PanSTARRS surveys on the brighter end.

Three APASS data releases were published after the official release of UCAC4: DR7, DR8, and DR9 (July 29, 2015), which in principle should have improved both the completeness and the photometric accuracy of the APASS survey. We merged UCAC4 and APASS DR8 to test this assumption and actually found the opposite: by matching the resulting catalog with a set of photometric standards it is easy to see that the photometric homogeneity is much worse with respect to APASS DR6. This is easily explained by some problems, which occurred during the DR7–DR9 observing campaigns and described in the release notes, which include the “blue” camera malfunctions in the Northern hemisphere and the “red” camera’s poor focus in the Southern hemisphere. Many of these problems are expected to be solved in the forthcoming DR10; meanwhile, we adopt the DR6 magnitudes throughout the present paper.

As a further step, we truncated UCAC4 at $V < 10$, where APASS photometry saturates, and replaced those entries with the corresponding photometry and proper motions from Tycho-2, converting Tycho (B_T, V_T) to Johnson (B, V) through the standard transformations given by Høg et al. (2000). During this process we identified 176 662 UCAC4 entries at $V > 10$ for which the tabulated B, V magnitudes were mistakenly copied from Tycho-2 (B_T, V_T) without any transformation; we fixed these entries by forcing the correct transformations as above. Finally, APASS magnitudes are not complete down to $f_{\text{mag}} = 13.5$ on some particular regions of the northern sky, so for those missing entries we calibrated UCAC4 f_{mag} and 2MASS J and K against the most recent set of secondary $UBVRI$ photometric standards

published by P. B. Stetson⁸ obtaining:

$$\begin{cases} B = f_{\text{mag}} + 1.8372(J - K) + 0.0627 & (\sigma = 0.15) \\ V = f_{\text{mag}} + 0.5659(J - K) - 0.1204 & (\sigma = 0.09) \end{cases} \quad (2)$$

where the RMS scatter around the best fit is calculated within the range of interest $10 < V < 13$.

The resulting catalog, trimmed at $f_{\text{mag}} < 13.5$ to be more easily manageable, will be called UCAC4-RPM hereafter. Even taking into account color effects in $V - f_{\text{mag}}$, this sample is magnitude-complete at $V < 13$ for FGK spectral types, and constitutes a perfect basis to cherry-pick targets for space-based exoplanet transit search missions such as TESS and PLATO. Coincidentally, $V = 13$ is also the typical limiting magnitude of the most fruitful wide-field, ground-based transit searches, making our effort of more general use. The overall number of UCAC4-RPM entries is 10 198 407, of which 9 928 389 have at least proper motions and B, V photometry either from Tycho2 or from APASS.

RAVE DR4 lists 425 561 stars, of which 412 741 are in common with UCAC4-RPM. 375 203 of them have valid proper motions, B, V magnitudes, and atmospheric parameters. The latter subset consists of stars which share a reliable estimate of $\log g$ and T_{eff} from RAVE ($\Delta \log g \simeq 0.3$ dex, $\Delta T_{\text{eff}} \simeq 150$ K on average), span the full range of Galactic latitude and perfectly overlap the typical magnitude range of our stellar sample. In other words, this is an ideal training set to calibrate RPM-based selections on the whole UCAC4-RPM.

4.2 Defining the RPM selection

Before selecting stars according to their RPMs, one has to choose which photometric bands to employ for the color (horizontal axis of the RPMD) and the RPM itself (vertical axis). While the proper motion of a given UCAC4-RPM entry is unique, two or three magnitudes have to be chosen from B, V, J, K , the latter two originating from 2MASS and included in UCAC4-RPM through UCAC4.

We ran several tests to see the impact of this choice on the ability of the RPMD to properly separate the main sequence from the evolved stars: the resulting RPMD for four different test choices, namely ($B - V, \text{RPM}(V)$), ($J - K, \text{RPM}(J)$), ($J - K, \text{RPM}(V)$), ($V - J, \text{RPM}(V)$) are plotted in Fig. 3, where the $\log g$ from RAVE is color-coded from 0.0 (blue) to 5.0 dex (red). At first sight, when integrating the results over the whole sky, all four choices are effective in separating the two “bumps” corresponding to main-sequence stars (centered approximately on unevolved F dwarfs) and red giants. However, the ($B - V, \text{RPM}(V)$) diagram performs better at low Galactic latitudes, where interstellar extinction plays a crucial role on the most distant stars. This is easily explained by the fact that $B - V$ is the color most affected by extinction. While nearby, late-type main-sequence dwarfs share a negligible or very small extinction, distant stars (which are mostly contaminating giants) are moved farther from the main sequence by the reddening vector, making the dwarf/giant separation easier. For this reason,

⁷ <https://www.aavso.org/apass>

⁸ <http://www.cadc-ccda.hia-ihh.nrc-cnrc.gc.ca/en/community/STETSON/standards/>

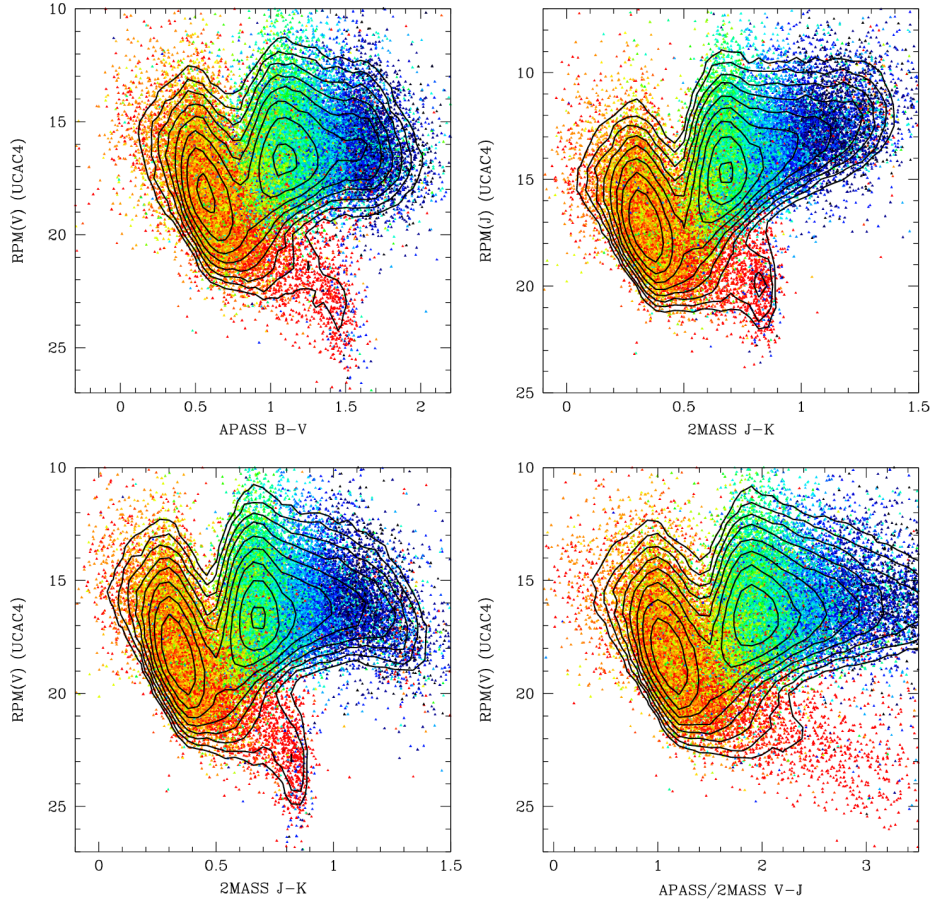


Figure 3. Reduced proper-motion diagrams for all the UCAC4-RPM sources in common with RAVE DR4, plotted by adopting different permutations of magnitudes: $(B - V, RPM(V))$, $(J - K, RPM(J))$, $(J - K, RPM(V))$, $(V - J, RPM(V))$ in reading order. The number of points are randomly decreased by a factor of ten to improve clarity, while the isodensity contours (black lines) are evaluated on the full sample. The $\log g$ values from RAVE are color coded within the range from 0.0 (deep blue) to 5.0 dex (pure red).

we adopted the $(B - V, RPM(V))$ plane to perform the following RPM calibrations and selections.

While one could in principle draw an empirical boundary line between giants and dwarfs on the RPMD by hand (as done, among others, by Gould & Morgan 2003), a more rigorous and quantitative approach is advisable when working with precise requirements on SpT (or, equivalently, on T_{eff} and $\log g$) as in our case. We first subdivided the RPMD plotted with all the stars in common between UCAC4-RPM and RAVE into small rectangular cells having side lengths equal to $\Delta(B - V) = 0.05$ mag and $\Delta RPM(V) = 0.5$ mag (unfilled circles in Fig. 4, left panels). Each star in a given cell is classified as a genuine DLF5/DSL5 target, or as a contaminant, according to its RAVE T_{eff} , $\log g$ based on the $T_{\text{eff}} < 6510$ K, $\log g > 4.0$ (DLF5) or $T_{\text{eff}} < 6510$ K, $\log g > 3.5$ (DSL5) criterion. The fraction Φ of genuine targets over contaminants is then evaluated for each cell. After some trial-and-error attempts, we define those cells having $\Phi > 50\%$ as “good”, though this threshold can be changed depending on whether one desires to increase the completeness (lower Φ threshold) or to decrease the contamination

(higher Φ) of the final sample. Cells in Fig. 4 are drawn as blue circles if $\Phi > 50\%$, and green otherwise. As a final step, with the aim of speeding up the computation, we approximated our RPM selection encompassing “good” cells through a polynomial chain (red line in Fig. 4), corresponding to the following cuts:

$$\begin{aligned}
 &RPM(V) > 12 \text{ and } (\\
 &[(B - V) > 0.7 \text{ and } RPM(V) > 19.75] \text{ or } \\
 &[(B - V) < 0.7 \text{ and } RPM(V) > 18.75] \text{ or } \\
 &[RPM(V) > (-10 + 33(B - V)) \text{ and } (B - V) > 0.438])
 \end{aligned} \tag{3}$$

for the DLF5 selection and

$$\begin{aligned}
 &RPM(V) > 10 \text{ and } (\\
 &[(B - V) > 0.7 \text{ and } RPM(V) > 19.5] \text{ or } \\
 &[(B - V) < 0.7 \text{ and } RPM(V) > 19.0] \text{ or } \\
 &[RPM(V) > (2 + 16(B - V)) \text{ and } (B - V) > 0.40])
 \end{aligned} \tag{4}$$

for the DSL5 selection; the “and” and “or” logical operators have their usual meaning.

Eq. 3 and 4 can be applied to the full UCAC4-

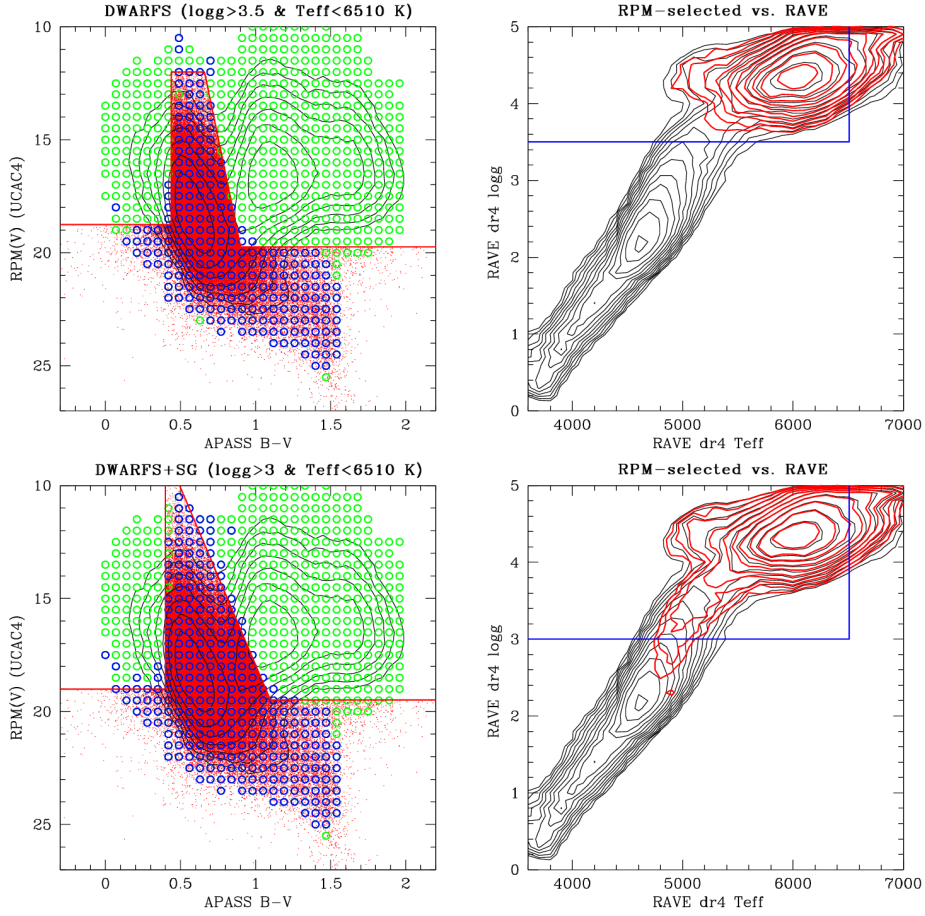


Figure 4. Procedure to extract DLF5 (upper panels) and DSLF5 (lower panels) stars from UCAC4-RPM according to their color and RPM. *Left panels:* Reduced proper-motion diagrams for a subset of stars in common between RAVE DR4 and UCAC4-RPM. Both RPMs are subdivided into cells (unfilled circles). The stars in each cell are classified as genuine DLF5/DSLF5 targets or as contaminants according to their RAVE T_{eff} , $\log g$; then the cell is drawn in blue if at least 50% of them are bona-fide DLF5/DSLF5 sources, and green otherwise. Our RPM selection encompassing “good” cells is approximated by a red polynomial chain, corresponding to the Eq. 3 and 4 numerical cuts. *Right panels:* effective temperature T_{eff} and surface gravity $\log g$ from RAVE DR4 for all stars in common with UCAC4-RPM (black contours), and after the RPM selection devised for the DLF5/DSLF5 sample is applied (red contours). The blue lines mark the boundaries $T_{\text{eff}} < 6510 \text{ K}$, $\log g > 3.5$ (DLF5) or $T_{\text{eff}} < 6510 \text{ K}$, $\log g > 3.0$ (DSLF5); red points outside these regions are therefore classified as contaminants (see text; compare with Fig. 2 and Table 1).

RPM sample to get whole-sky, magnitude-limited samples of DLF5 and DSLF5 stars. For instance, the DLF5 subset contains 84 432, 287 914, 899 761, 2 627 966 entries at $V < 10, 11, 12, 13$, respectively. A more detailed summary of the UCAC4-RPM star counts as a function of V magnitude and $B - V$ color is tabulated on Table 2. The full UCAC4-RPM catalog, augmented with a flag about the DLF5/DSLF5 RPM-based classification, is made publicly available through Vizier and a dedicated web server⁹.

4.3 Estimating completeness and contamination

To estimate the completeness and contamination of our UCAC4-RPM classifications, following the same approach

applied in Section 3.3, we can put our subsamples into the RAVE DR4 $\log g$ vs. T_{eff} diagram to check how many points lie in the allowed DLF5/DSLF5 region *a posteriori*, and how many of the RAVE DR4 dwarfs are effectively selected as such by our algorithm. The results are tabulated in Table 1. Our approach results in a comparable amount of contamination ($\approx 28\%$) and much better completeness ($\approx 80\%$) with respect to the previous classification attempts (AM06, OF08), i.e. we end up with a much cleaner sample of dwarfs and subgiants at a fainter limiting magnitude. This result is probably close to the intrinsic limit of the RPM technique, which is a statistical method.

In principle, every photometric classification technique is expected to worsen its performances when moving to the densest regions, i.e., close to the Galactic plane. The first reason is because crowding impacts the accuracy of the input

⁹ <http://groups.dfa.unipd.it/ESPG>

Table 2. DLF5/DSL5 star counts from UCAC4-RPM as a function of V magnitude (left table) and $B - V$ color (right table), along with the corresponding areal density $N(\square)$, spectral types SpT, absolute magnitude M_V , effective temperature T_{eff} , limiting distance d_{lim} at the limiting magnitude $V = 13$.

V	DLF5	$N(\square)$ [deg $^{-2}$]	DSL5	$N(\square)$ deg $^{-2}$	$B - V$	DLF5	$N(\square)$ deg $^{-2}$	SpT	M_V	T_{eff} [K]	d_{lim} [pc]
<8.0	4422	0.10	5818	0.14	<0.45	53749	1.57	F5V	3.40	6510	831
8.0-8.5	4995	0.12	6413	0.16	0.45-0.50	178269	5.22	F6V	3.70	6340	724
8.5-9.0	11511	0.27	14059	0.34	0.50-0.55	243253	7.13	F8V	4.01	6170	628
9.0-9.5	21248	0.51	25789	0.62	0.55-0.60	276979	8.12	G0V	4.45	5920	513
9.5-10.0	42244	1.02	50703	1.22	0.60-0.65	266499	7.81	G2V	4.79	5770	438
10.0-10.5	71459	1.73	86216	2.08	0.65-0.70	235501	6.90	G4V	4.94	5680	409
10.5-11.0	131750	3.19	155236	3.76	0.70-0.75	179495	5.26	G8V	5.32	5490	343
11.0-11.5	227458	5.51	266026	6.44	0.75-0.80	129239	3.79	G9V	5.55	5340	309
11.5-12.0	383479	9.29	445153	10.7	0.80-0.85	87223	2.55	K0V	5.76	5280	280
12.0-12.5	647860	15.7	746631	18.0	0.85-0.90	43033	1.26	K2V	6.19	5040	230
12.5-13.0	1077810	26.1	1235974	29.9	>0.90	91697	2.68	K4V	7.04	4620	156

Notes. The left table lists counts from the whole UCAC4-RPM catalog. The right table is extracted from a subset trimmed at $|b| > 10^\circ$ and $V < 13$ as described in Sec. 4.4, to be strictly magnitude-limited, and to avoid the regions close to the Galactic plane where the contamination rate on the latest spectral types is higher. The quantities SpT, M_V , T_{eff} are the average of each bin calculated through the SpT/ T_{eff} calibration by E. Mamajek described in Sec. 2.

catalogs. This could be an issue for APASS (our primary source of optical magnitudes at $V > 10$), because the pixel scale of that survey is 2.57 arcsec/pixel, and the PSFs were deliberately defocused to a FWHM of 1.5-2.0 pixels. On the other hand, our targets are relatively bright ($V < 13$) and only marginally affected by confusion down to a few degrees from the Galactic plane. A second reason is that lines of sight at low Galactic latitudes can reach very high values of interstellar extinction as the distance increases, therefore early-type stars can be misidentified as later-type dwarfs. This effect is larger at the faint end of the sample, which probes a larger volume of space. But this is counterbalanced by another effect which actually improves the giant/dwarf separation on very reddened lines of sight: evolved stars are moved farther from the main sequence on the RPMD, as explained in Sec. 4.2.

To assess how much the proximity to the Galactic plane could be a limiting factor to our classification, we redid the completeness/contamination estimate as above by selecting UCAC4-RPM stars within three different ranges of Galactic latitudes: $|b| < 10$, $10 < |b| < 20$, and $|b| > 20$ (Table 1). The results are pretty clear: on average, the efficiency of our algorithm is not significantly impacted by b . The contamination level is remarkably constant at $\approx 28\%$, while completeness actually improves a bit toward the Galactic plane, from $\approx 71\%$ to $\approx 81\%$. By looking at an all-sky chart of DSL5 stars (Fig. 5), it is easy to notice that their surface density increases by a factor of two to three from the Galactic poles to the disk, as predicted by stellar models such as TRILEGAL or Besançon Galactic models (Girardi et al. 2005; Robin et al. 2003) for DSL5 stars. The only exception is the presence of a few overdensities at very low b (blue regions in Fig. 5), where the fraction of false positives is much larger than 30%. These regions, however, cover only a negligible fraction of the sky and therefore do not significantly contribute to the overall statistics.

4.4 Comparison with Galactic models

As a further validation of our catalog, we made a more detailed comparison between UCAC4-RPM and GUMS (Gaia Universe Model Snapshot; Robin et al. 2012) an all-sky synthetic catalog based on an updated version of the Besançon Galactic model (BGM; Robin et al. 2003) and aimed to a realistic simulation of the Gaia performances. Such analysis should be regarded not only as a validation check for UCAC4-RPM, but also as a test for the BGM and its underlying assumptions, the most relevant of which for our purposes is the luminosity function of the Solar neighborhood (Reid et al. 2002). UCAC4-RPM is a magnitude-limited sample, as opposed to a volume-limited one, so the local luminosity functions must be first convolved by a Galactic model to get a meaningful comparison. It is worth noting that, at the faint limit considered here, UCAC4-RPM is probing heliocentric distances up to ~ 830 pc (assuming $M_V(\text{F5V}) = 3.4$ at $V = 13$), with a median distance of ~ 300 pc for a typical Sun-like star ($M_V(\text{G2V}) = 4.8$ at $V = 12.1$). As a reference, the Reid et al. (2002) luminosity function is based on a Hipparcos sample volume-limited at 25 pc.

Both UCAC4-RPM and GUMS were first cut at $V < 13$ (where UCAC4-RPM is complete), then only the DLF5 stars were selected by imposing $\log g > 3.5$ and $T_{\text{eff}} < 6510$ K following our definition in Sec. 3.3. In order to perform a fair comparison, a further cut was set at $|b| > 10^\circ$ to exclude regions close to the Galactic plane, where extinction maps (including that by Drimmel et al. 2003 implemented by GUMS) are known to be unreliable in reproducing the observed stellar counts (Marshall et al. 2006; Schultheis et al. 2014). The resulting histogram as a function of T_{eff} is shown in Fig. 6

The total number of UCAC4-RPM DLF5 dwarfs at $V < 13$ and $|b| < 10^\circ$ is 1770693, that is 21% more than the 1460174 predicted by GUMS. This is a reasonable agreement after considering that the overall contamination rate of UCAC4-RPM is estimated to be at about 28% (Table 1). A closer look to Fig. 6 reveals that while the counts for the F0-F5 subsample ($T_{\text{eff}} > 5908$ K) are essentially identical in the

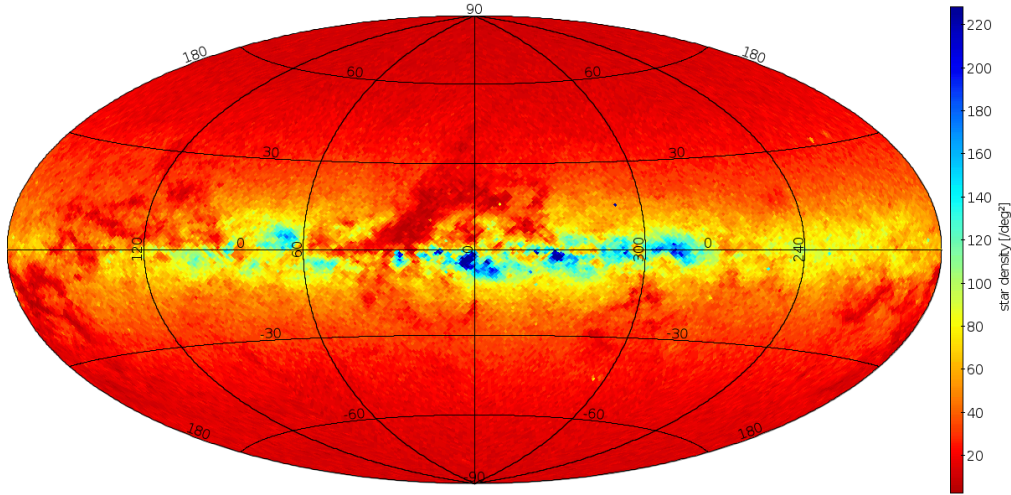


Figure 5. All-sky chart of our UCAC4-RPM catalog, DSLF5 subset. Areal density is linearly color-coded from 30 deg^{-2} (pure red) to 80 deg^{-2} (pure yellow) and 220 deg^{-2} (deep blue). Star density varies within a factor of 2-3 as a function of Galactic latitude, as predicted by Galactic models, except for a few regions at $|b| \lesssim 5$ where extreme amounts of crowding and/or interstellar extinction boost the fraction of false positives (See Sec. ??). The underdense regions at $l = 0^\circ\text{-}30^\circ, b = 0^\circ\text{-}20^\circ$ and $l \sim 175^\circ, b \sim -15^\circ$ are the Serpens/Aquila/Ophiucus rift and the Taurus complex, respectively (Cambr esy 1999).

two catalogs (598 194 vs. 617 643, -3.1%), the stars in excess in UCAC4-RPM come from the G ($5310 < T_{\text{eff}} < 5908 \text{ K}$, 879 558 vs. 638 652, $+37\%$) and K subsets ($T_{\text{eff}} < 5310 \text{ K}$, 292 941 vs. 199 315, $+47\%$). This is consistent with the hypothesis that the excess counts come from contaminating subgiants, since they are predicted to belong mostly to the G and K spectral types (see Fig. 4, right panels). Summarizing, the UCAC4-RPM results seem to be in a generally good agreement with the current models of the Solar neighborhood and their assumptions.

5 POSSIBLE APPLICATIONS OF UCAC4-RPM FOR EXOPLANET SEARCHES

UCAC4-RPM is nicely suited to build a preliminary input catalog for future space-based missions, like TESS and PLATO, as well as ongoing and forthcoming ground-based surveys.

5.1 TESS

With its four wide-field optical cameras pointed toward different lines of sight, TESS will simultaneously monitor a $24^\circ \times 94^\circ$ strip (i.e., 2300 deg^2) for 27 days, then it will take a 26° turn around the Ecliptic pole and repeat this cycle in order to scan nearly the full sky at Ecliptic latitude $|\beta| > 6^\circ$ during its two-year nominal mission (Ricker et al. 2015). The temporal coverage will therefore range from 27 d at low ecliptic latitudes, to about 1 year over 900 deg^2 close to the ecliptic poles.

The prime targets for TESS are main-sequence dwarfs from F5 to M5; photon noise and confusion set the limiting magnitude at $I_c \simeq 12$, or roughly $V \simeq 13$ at K2V. While TESS will transmit the full-frame images back to Earth with a 30-min cadence, a highest-priority subset of $\sim 200\,000$ pre-selected stars will be monitored at a cadence of 2 min. Being

magnitude limited at $V \lesssim 13.5$ and focused on DLF5 stars, UCAC4-RPM is perfectly suited to support the TESS target selection. It provides a sample of $\sim 2\,600\,000$ $V < 13$ dwarfs from which the TESS target list can be cherry-picked according to a prioritization scheme based on the expected transit detection efficiency. Such an approach should be regarded as complementary to that developed by the TESS Target Selection Working Group (TWSG), which is in charge of building the TESS Target Catalog (TTC; Stassun et al. 2014). The TTC is based on a different combination of input catalogs with respect to UCAC4-RPM, and on different selection algorithms and thresholds.

While the full TTC has not been released to the community yet, a public subset of it covering the K2 fields is named K2-TESS and documented by Stassun et al. (2014). K2-TESS allows us to probe the overlap region between our catalog and the TTC. If, for instance, we cross-match the K2 ‘‘Campaign 2’’ field with UCAC4-RPM, we get 5 662 DSLF5 (of which 4 726 are DLF5). Among these, 565 UCAC4-RPM dwarfs are missed by K2-TESS, while there are 2 234 K2-TESS dwarfs missed by UCAC4-RPM, mostly because of their faintness ($V > 13.5, J > 11.5$). This is somewhat expected since the two catalogs are based on different methodologies and input catalogs reflecting different scientific priorities. While K2-TESS is more focused on cool SpTs (late K and M dwarfs) and mainly based on the 2MASS infrared photometry, UCAC4-RPM is focused on solar-type FGK targets, implying different selection algorithms and thresholds. In other words, the two approaches will be highly synergic in selecting the optimal targets for TESS (Stassun et al. 2014).

5.2 PLATO

The unique optical design of PLATO (Rauer et al. 2014) is driven by the requirement to cover a significant fraction of the sky with a good image quality in order to achieve an

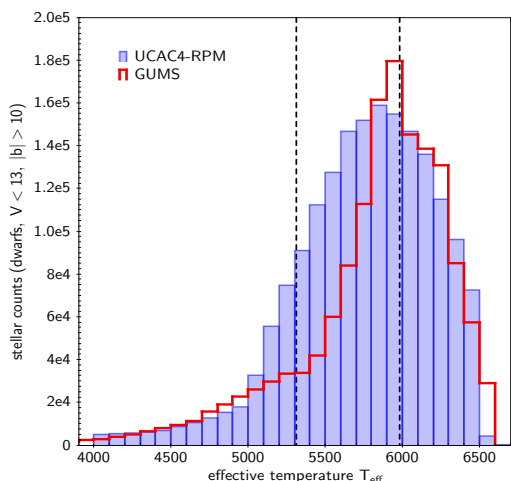


Figure 6. Histogram comparing the temperature distribution of a magnitude-limited sample of dwarf stars from UCAC4-RPM (this work; blue bars) and from the GUMS simulated catalog (Robin et al. 2012; red bars) based on the Besancon Galactic model (Robin et al. 2003). Both samples are cut at $V < 13$ and $|b| > 10^\circ$. The two dashed vertical lines mark the boundary between G/K and F/G main-sequence spectral types, respectively.

unprecedented photometric precision: < 34 ppm/h (parts per millions measured over a 1-hour time scale) for the main scientific sample limited at $V < 11$, and even better for the brightest stars of the sample at $V \simeq 6$ (dominated by systematic errors). The present design of PLATO implies that the array of 12-cm telescopes is subdivided into four groups, each group pointing towards a direction which is displaced by an angle $\theta = 9.2$ deg from the center of the overall field of view (FOV). Such strategy provides a non-uniform instantaneous coverage of a 2124 deg^2 field.

The observing strategy of PLATO consists of a two-step approach in order to maximize the scientific return of the mission. PLATO will image two “long-duration” (LD) fields for more than two years each, and some supplementary fields for a few months each, during the “step & stare” (S&S) phase. The LD phase will fulfil the main scientific objective of the mission, being sensitive to planets down to the Earth’s size orbiting within the habitable zone (HZ) of solar-type (FGK) stars. The S&S fields will expand the accessible sky area by about one order of magnitude, giving us access to a larger number of bright nearby stars at the expense of probing a smaller range of orbital periods. A simple calculation shows that, at the end of a nominal 6.5-year mission with 2 LD and 10 S&S fields, PLATO will have surveyed about two thirds of the whole sky.

The PLATO Science Requirements Document¹⁰ (SRD) defines five complementary stellar samples to be surveyed, listed in decreasing priority and summarized below:

- P1: DSLF5 stars brighter than $V = 11$, monitored with a photometric noise level $\sigma \leq 34$ ppm/h, to be observed during the LD phase;
- P2, P3: DSLF5 stars brighter than $V = 8$, monitored at $\sigma \leq 34$ ppm/h, to be observed during the LD and S&S phase, respectively.

- P4: cool M dwarfs (M0 or later), to be monitored during the LD phase of the mission (at $V < 16$), or during the S&S phase (at $V < 15$). The photometric noise level for both subsamples must be below 800 ppm/h;
- P5: DSLF5 stars brighter than $V = 13$, to be observed during the LD phase.

Samples P1, P2, P3, P5 are therefore all made of “solar-like” stars brighter than $V = 13$. Due to telemetry limitations, PLATO will not be able to download the full images, collected with cadence between 60 s (normal telescopes) and 2.5 s (for the two “fast” telescope, dedicated to bright stars, and the only ones equipped with two filters, for color measurement). Only for a limited subsample of targets it will be possible to download imaggettes. Most of the photometry must be done on board on the selected targets, and also the imaggette centers must be pre-selected. In other words, PLATO needs an input catalog (PIC: PLATO Input Catalog). It is clear that our new UCAC4-RPM represents the most appropriate tool to preliminarily select and prioritize the target sample. It also is of basic importance for a selection of PLATO fields, needed, for engineering reasons, well before GAIA catalogs can be used.

5.3 Ground-based surveys

UCAC4-RPM is made publicly available to the astronomical community. Its magnitude range $6 \lesssim V \lesssim 13$ makes it exploitable for the ongoing ground-based transit surveys such as SuperWASP/WASP South (Pollacco et al. 2006; Hellier et al. 2011), HatNet/Hat-South (Bakos et al. 2009b,a), KELT/KELT-South (Pepper et al. 2007, 2012) or NGTS (Chazelas et al. 2012) to vet and prioritize the list of planetary candidates and to discard transit-like signals originating from early-type or giant stars, when no other source of reliable stellar parameters is available. A careful preliminary characterization of the target stars has been proven to greatly speed up the follow-up process, avoiding a loss of observing time and resources by monitoring false positives (Almenara et al. 2009; Bryson et al. 2013).

6 CONCLUSIONS

Throughout the previous sections, we described how we devised a new RPM-based algorithm to assign a luminosity class to field stars by knowing only their proper motions and two optical magnitudes. By applying this optimal algorithm on a new stellar catalog compiled by matching UCAC4, APASS DR6 and Tycho-2, we ended up with UCAC4-RPM—an all-sky sample of solar-type dwarf stars complete down to at least $V \simeq 13$. We demonstrated that the latter catalog, once complemented by subgiants within the same spectral type range, meets the requirements set by the PLATO team for the target selection of its main stellar samples. In particular, the relatively low level of contamination ($\lesssim 30\%$) of UCAC4-RPM, together with a $\gtrsim 80\%$ completeness, is well suited to PLATO (but also TESS), whose telemetry allows us to select many more targets with respect to the nominal requirement of P1 stars, therefore compensating for the fraction lost due to contaminants. UCAC4-RPM proved to be

¹⁰ ID code: ESA-PLATO-ESTEC-SCI-RS-001.

helpful as a starting point to select the (provisional) coordinates of the long-duration pointing fields, which are needed at this stage to tune the observational strategy, to run engineering tests and to plan an optimal follow-up strategy for the object of interest to be delivered by PLATO. Also ongoing and forthcoming ground-based survey for exoplanet search may benefit by UCAC4-RPM catalog.

It is possible to take future steps to improve UCAC4-RPM. The most obvious one is the inclusion of newer releases of APASS, to rely on a more accurate, complete and homogeneous source of B and V magnitudes. APASS DR8 and DR9 are already available, but both suffer from photometric inhomogeneity due to the inclusion of more recent data and a filter change; it is expected that APASS DR10, still to be released, will solve most of these problems. Additionally the training set used in the present work (RAVE) could be improved by including other wide-field spectroscopic surveys, such as SDSS/SEGUE (Yanny et al. 2009) and especially LAMOST/LEGUE (Deng et al. 2012), which will enable us to calibrate our RPM selections on both hemispheres (RAVE is limited to $b \leq 0$) and to fainter magnitudes, i.e., including more dwarfs of K and M spectral types. We performed a preliminary cross-check by mapping the surface gravity listed on the first public release of LAMOST (DR1) on the full UCAC4-RPM sample. As expected, the LAMOST parameters confirm the accuracy of our previous dwarf vs. giant separation on the RPM diagram based on RAVE (Fig. 4). Once the first LAMOST complete release will be made available to the community, we expect to increase the size of our training set by a factor of ten.

The Gaia final catalog, to be released no earlier than 2024, is expected to make UCAC4-RPM obsolete on most of the sky, thanks to its accurate spectrophotometric measurements (BP/RP instrument) and exquisitely precise geometrical parallaxes (ASTRO instrument). However, the algorithms on which UCAC4-RPM is based could help in exploiting the Gaia data to estimate luminosity classes at $V > 11$ much earlier than 2024, starting from the second intermediate release (DR2; end of 2017), when just BP/RP integrated magnitudes and proper motions will be available, but not distances or surface gravities. A modified version of the algorithm presented in Section 4 can be easily adapted and calibrated through LAMOST+RAVE to work in the ($G_{BP} - G_{RP}$, RPM(G)) plane.

ACKNOWLEDGEMENTS

V. N. and G. P. acknowledge partial support by the Università di Padova through the “progetto di Ateneo #CPDA103591”, and by the Agenzia Spaziale Italiana (ASI) through the contract PLATO. V. N. acknowledges partial support from INAF-OAPd through the grant “Analysis of HARPS-N data in the framework of GAPS project” (#19/2013) and “Studio preparatorio per le osservazioni della missione ESA/CHEOPS” (#42/2013). The present work has been carried out following the ASI-INAF agreement num. 2015-019-R0, 2015 July 29.

REFERENCES

Almenara J. M., et al., 2009, *A&A*, **506**, 337

- Ammons S. M., Robinson S. E., Strader J., Laughlin G., Fischer D., Wolf A., 2006, *ApJ*, **638**, 1004
- Árnadóttir A. S., Feltzing S., Lundström I., 2010, *A&A*, **521**, A40
- Bailer-Jones C. A. L., 2010, *MNRAS*, **403**, 96
- Bailer-Jones C. A. L., 2011, *MNRAS*, **411**, 435
- Bailer-Jones C. A. L., et al., 2013, *A&A*, **559**, A74
- Bakos G. Á., et al., 2009a, in Pont F., Sasselov D., Holman M. J., eds, IAU Symposium Vol. 253, IAU Symposium. pp 21–27, doi:10.1017/S1743921308026197
- Bakos G., et al., 2009b, in Pont F., Sasselov D., Holman M. J., eds, IAU Symposium Vol. 253, IAU Symposium. pp 354–357, doi:10.1017/S174392130802663X
- Batalha N. M., et al., 2010, *ApJ*, **713**, L109
- Belikov A. N., Röser S., 2008, *A&A*, **489**, 1107
- Bessell M. S., 2005, *ARA&A*, **43**, 293
- Bressan A., Marigo P., Girardi L., Salasnich B., Dal Cero C., Rubele S., Nanni A., 2012, *MNRAS*, **427**, 127
- Brown T. M., Latham D. W., Everett M. E., Esquerdo G. A., 2011, *AJ*, **142**, 112
- Bryson S. T., et al., 2013, *PASP*, **125**, 889
- Cambrésy L., 1999, *A&A*, **345**, 965
- Chazelas B., et al., 2012, in Society of Photo-Optical Instrumentation Engineers (SPIE) Conference Series. , doi:10.1117/12.925755
- Cox A. N., 2000, Allen’s astrophysical quantities
- Deleuil M., et al., 2006, in Fridlund M., Baglin A., Lochard J., Conroy L., eds, ESA Special Publication Vol. 1306, The CoRoT Mission Pre-Launch Status - Stellar Seismology and Planet Finding. p. 341
- Deleuil M., et al., 2009, *AJ*, **138**, 649
- Deng L.-C., et al., 2012, *Research in Astronomy and Astrophysics*, **12**, 735
- Drimmel R., Cabrera-Lavers A., López-Corredoira M., 2003, *A&A*, **409**, 205
- Fischer D. A., et al., 2005, *ApJ*, **620**, 481
- Girardi L., Groenewegen M. A. T., Hatziminaoglou E., da Costa L., 2005, *A&A*, **436**, 895
- Gontcharov G. A., 2009, *Astronomy Letters*, **35**, 638
- Gould A., Morgan C. W., 2003, *ApJ*, **585**, 1056
- Hambly N. C., et al., 2001, *MNRAS*, **326**, 1279
- Hellier C., et al., 2011, in European Physical Journal Web of Conferences. p. 1004 (arXiv:1012.2286), doi:10.1051/epjconf/20101101004
- Henden A., Munari U., 2014, Contributions of the Astronomical Observatory Skalnaté Pleso, **43**, 518
- Hertzprung E., 1922, Bull. Astron. Inst. Netherlands, **1**, 91
- Høg E., et al., 2000, *A&A*, **355**, L27
- Kapteyn J. C., van Rhijn P. J., 1920, *ApJ*, **52**, 23
- Kordopatis G., et al., 2013, *AJ*, **146**, 134
- Lépine S., Shara M. M., 2005, *AJ*, **129**, 1483
- Marshall D. J., Robin A. C., Reylé C., Schultheis M., Picaud S., 2006, *A&A*, **453**, 635
- Morgan W. W., Keenan P. C., 1973, *ARA&A*, **11**, 29
- Nordström B., et al., 2004, *A&A*, **418**, 989
- Ofek E. O., 2008, *PASP*, **120**, 1128
- Pecaut M. J., Mamajek E. E., 2013, *ApJS*, **208**, 9
- Pepper J., et al., 2007, *PASP*, **119**, 923
- Pepper J., Kuhn R. B., Siverd R., James D., Stassun K., 2012, *PASP*, **124**, 230
- Perryman M. A. C., ESA eds, 1997, The HIPPARCOS and TYCHO catalogues. Astrometric and photometric star catalogues derived from the ESA HIPPARCOS Space Astrometry Mission ESA Special Publication Vol. 1200
- Perryman M. A. C., et al., 2001, *A&A*, **369**, 339
- Pickles A. J., 1998, *PASP*, **110**, 863
- Pickles A., Depagne É., 2010, *PASP*, **122**, 1437
- Pollacco D. L., et al., 2006, *PASP*, **118**, 1407
- Rauer H., et al., 2014, *Experimental Astronomy*, **38**, 249

- Recio-Blanco A., et al., 2016, *A&A*, **585**, A93
- Reid I. N., Gizis J. E., Hawley S. L., 2002, *AJ*, **124**, 2721
- Ricker G. R., et al., 2015, *Journal of Astronomical Telescopes, Instruments, and Systems*, **1**, 014003
- Robin A. C., Reyl e C., Derri ere S., Picaud S., 2003, *A&A*, **409**, 523
- Robin A. C., et al., 2012, *A&A*, **543**, A100
- Schultheis M., et al., 2014, *AJ*, **148**, 24
- Skiff B. A., 2014, VizieR Online Data Catalog, **1**, 2023
- Skrutskie M. F., et al., 2006, *AJ*, **131**, 1163
- Soubiran C., Le Campion J.-F., Cayrel de Strobel G., Caillo A., 2010, *A&A*, **515**, A111
- Stassun K. G., Pepper J. A., Oelkers R., Paegert M., De Lee N., Sanchis-Ojeda R., 2014, preprint, ([arXiv:1410.6379](https://arxiv.org/abs/1410.6379))
- Steinmetz M., et al., 2006, *AJ*, **132**, 1645
- Straizys V., Lazauskait e R., Brown A. G. A., Zdanavi cius K., 2006, *Baltic Astronomy*, **15**, 449
- Teig M., 2008, *PASP*, **120**, 474
- Valenti J. A., Fischer D. A., 2005, *ApJS*, **159**, 141
- Yanny B., et al., 2009, *AJ*, **137**, 4377
- Zacharias N., Monet D. G., Levine S. E., Urban S. E., Gaume R., Wycoff G. L., 2005, VizieR Online Data Catalog, **1297**, 0
- Zacharias N., Finch C. T., Girard T. M., Henden A., Bartlett J. L., Monet D. G., Zacharias M. I., 2013, *AJ*, **145**, 44
- Zdanavi cius K., 1998, *Baltic Astronomy*, **7**, 551
- Zdanavi cius K., 2005, *Baltic Astronomy*, **14**, 104
- van Altena W. F., 2011, in *Revista Mexicana de Astronomia y Astrofisica Conference Series*. pp 290–290
- van Leeuwen F., 2007, *A&A*, **474**, 653

This paper has been typeset from a $\text{\TeX}/\text{\LaTeX}$ file prepared by the author.